Geophysical Research Letters

RESEARCH LETTER
10.1029/2023GL104583

# The Quasi-Linear Absolute Angular Momentum Slope of Tropical Cyclones Under Rapid Intensification

**Dandan Tao[1,2], Robert Nystrom[3], and Michael Bell[2]**

[1]University of Bergen, Bergen, Norway, [2]Colorado State University, Fort Collins, CO, USA, [3]National Center for Atmospheric Research, Boulder, CO, USA

**Key Points:**

- The slope of $M$ outside of $r_m$ is found to be quasi-linear in the inner core during rapid intensification
- The normalized quasi-linear $M$ slope flattens with increasing intensity
- The quasi-linear $M$ slope enables a simple reconstruction of tropical cyclone inner-core wind profiles

**Correspondence to:**

D. Tao,
ddantao@gmail.com

**Citation:**

Tao, D., Nystrom, R., & Bell, M. (2023). The quasi-linear absolute angular momentum slope of tropical cyclones under rapid intensification. *Geophysical Research Letters*, *50*, e2023GL104583. https://doi.org/10.1029/2023GL104583

Received 20 MAY 2023
Accepted 3 AUG 2023

**Author Contributions:**

**Conceptualization:** Dandan Tao, Michael Bell
**Formal analysis:** Dandan Tao, Robert Nystrom
**Investigation:** Dandan Tao, Robert Nystrom
**Methodology:** Dandan Tao, Michael Bell
**Resources:** Michael Bell
**Validation:** Dandan Tao, Robert Nystrom
**Writing – original draft:** Dandan Tao, Robert Nystrom
**Writing – review & editing:** Dandan Tao, Robert Nystrom, Michael Bell



## Abstract

Tropical cyclone (TC) low-level tangential wind structure is known to be an important input for risk assessment (e.g., storm surge). However, a realistic TC wind structure model with easy implementation is still needed for many applications. In this study, we obtain an inner-core wind structure model purely from an empirical approach, which significantly reduces the complexity of TC wind profiles. From idealized simulations with different initial vortex structures, it is found that the absolute angular momentum ($M$) outside the radius of maximum wind ($r_m$) is quasi-linear. This quasi-linear $M$ slope in a normalized coordinate decreases with TC intensity. The consequent linear $M$ slope wind model can largely capture the simulated TC inner-core wind structure and has the potential for many practical applications.

## Plain Language Summary

In this study, we confirmed the quasi-linear characteristic of the absolute angular momentum outside the radius of maximum wind during rapid intensification. Through the analysis of the tangential (swirling) wind and absolute angular momentum, we showed that the evolution of inner-core tangential wind happens as the redistribution of the absolute angular momentum in the inner core. This redistribution does not change the quasi-linear characteristic of the absolute angular momentum. We further found that an increasing intensity is associated with a flattening absolute angular momentum slope during the rapid intensification period. The proposed quasi-linear absolute angular momentum wind model has great potential for many practical applications (e.g., risk management, model initialization and validation) as it enables a simple reconstruction of tropical cyclone tangential wind profiles given three minimal inputs of maximum tangential wind, radius of maximum wind and radius of gale force wind.

## 1. Introduction

A lot of efforts have been put into the estimation of tropical cyclone (TC) surface winds (Knaff et al., 2021). The current most widely used TC structural parameters are the maximum sustained wind, the radius of maximum wind, and the radius of gale force wind. However, to get a more accurate estimate of potential damage caused by severe TCs, a more complete radial structure of the tangential wind field is needed (Yan & Zhang, 2022). TC wind structure models are then built to fully represent wind profiles with little need of observation coverage (Chavas et al., 2015; Holland, 1980; Willoughby et al., 2006). However, many of these models suffer from complex formulas. A widely used simple TC wind structure model is the modified Rankine vortex (hereafter mRankine model),

$$V_t(r) = V_m \times \left(\frac{r_m}{r}\right)^{\alpha}, r \geq r_m \quad (1)$$

in which $V_t$ is the tangential wind, $V_m$ is the maximum tangential wind, $r_m$ is the radius of the maximum tangential wind and $\alpha$ is a tunable parameter to adjust wind decay outside of $r_m$. A larger $\alpha$ represents a skinnier wind skirt outside of $r_m$ for a strong vortex, while smaller $\alpha$ represents a broader wind skirt outside of $r_m$ for a weaker vortex (Mallen et al., 2005). Equation 1 achieves a continuous wind profile with very few inputs ($V_m$, $r_m$, and $\alpha$), which has been widely used in vortex initialization (Braun et al., 2012; Stern & Nolan, 2012; Rappin et al., 2013; Komaromi et al., 2021; Christophersen et al., 2022; etc.) and compared with observations (DeMaria et al., 2009; Knaff et al., 2016; Mallen et al., 2005). With $\alpha = 0.55$, it also turns out to be a good estimate for the mean TC structure for the 2004–2020 southwest Atlantic TC subset (Klotzbach et al., 2022).

A more recent wind structure model proposed by Chavas et al. (2015, hereafter C15 model) combines the wind structures from Emanuel and Rotunno (2011) inner core and Emanuel (2004) outer region. The merit of this

model is that it needs very few inputs to create a continuous profile all the way into the center and has a quite good match to observations especially for outer winds. It can also be used to estimate $r_m$ from $V_m$ and the radius of 17.5 $ms^{-1}$ wind (Chavas & Knaff, 2022). However, one disadvantage of this model lies in the equation for the inner-core wind profile (Equation 6 in C15),

$$\left(\frac{M}{M_m}\right)^{2-C_k/C_d} = \frac{2(r/r_m)^2}{2-(C_k/C_d)+(C_k/C_d)(r/r_m)^2}, \tag{2}$$

where $M = V_t r + \frac{1}{2} f r^2$ is the absolute angular momentum, $M_m$ is $M$ at $r_m$, $C_k$ is the enthalpy exchange coefficient and $C_d$ is the momentum exchange coefficient. Because of the steady state and balance assumptions (Emanuel & Rotunno, 2011), it does not allow for large variation in the inner-core wind structures and the calculation requires a constant $C_k/C_d$ ratio.

The above-mentioned wind structure models have shown some deficiencies or contain complicated equations. With the large variability in TC structure, efforts are still needed to reduce the dimensionality and complexity in describing a continuous radial profile of TC tangential wind.

Martinez et al. (2017) analyzed the Extended Flight Level Dataset for Tropical Cyclones and found that the normalized $M$ surfaces have a quasi-linear structure outside of $r_m$ (their Figure 9). This quasi-linear $M$ structure is also observed in the ensemble simulations of Hurricane Patricia (2015) in Tao et al. (2022) and the idealized simulations in Nystrom et al. (2020). Thus, we hypothesize that the quasi-linear $M$ slope outside of $r_m$ is valid for TCs with a dominant axisymmetric component (especially TCs undergoing RI). We define the slope in a normalized coordinate as

$$\mathrm{SL} = \left(\frac{M}{M_m} - 1\right) \Big/ \left(\frac{r}{r_m} - 1\right) = (M^* - 1)/(r^* - 1), r > r_m \tag{3}$$

where $M^* = \frac{M}{M_m}$ and $r^* = \frac{r}{r_m}$.

This slope is analogous to the angle ∅ defined in Casas et al. (2023) such that $\mathrm{SL} = \tan^{-1}(\varnothing)$. It is found in Casas et al. (2023) that the angle ∅ acts as an indicator of TC maturity; thus, we further hypothesize that SL magnitude changes with TC intensity.

In this quasi-linear $M$ slope wind model (hereafter, SL model), we can get $M^*$ easily from

$$M^* = \mathrm{SL} \times (r^* - 1) + 1, \tag{4}$$

while the value of SL can be determined by two points on the wind profile (e.g., point of maximum wind and point of gale force wind as they are often available in TC records).

Our hypotheses and the behavior of the SL model are tested herein using both idealized 3-dimensional TC simulations and Extended Best-Track (EBT) data set. Section 2 describes the model setup and the EBT data processing. Section 3 shows the results from the numerical model simulations, the wind model reconstructions and the EBT data set. The last section is the conclusion and discussion.

## 2. Methodology

### 2.1. Idealized Simulations

The Advanced Research version of the Weather Research and Forecast (ARW-WRF) model (version 3.9.1) is used for the simulations. There are three two-way nested model domains, with domain sizes of 5,400 km by 5,400 km (D1), 1,800 km by 1,800 km (D2), and 1,000 km by 1,000 km (D3), and horizontal grid spacings of 18, 6, and 2 km, respectively. The model has 41 vertical levels with the model top at 10 hPa. The two nested domains (D2 and D3) are moveable, with the domain center following the 850-hPa vortex center. The model uses the Yonsei University (YSU) boundary layer scheme (Hong et al., 2006) with a surface layer scheme of Dudhia et al. (2008), WRF single-moment 6-class microphysics (Hong & Lim, 2006), no cumulus parameterization and no radiation schemes. Non-SAL moist tropical sounding (Dunion & Marron, 2008) is used for the environmental moisture and temperature profiles with a constant sea surface temperature of 27°C and a constant Coriolis parameter $f = 5 \times 10^{-5}$ $s^{-1}$.

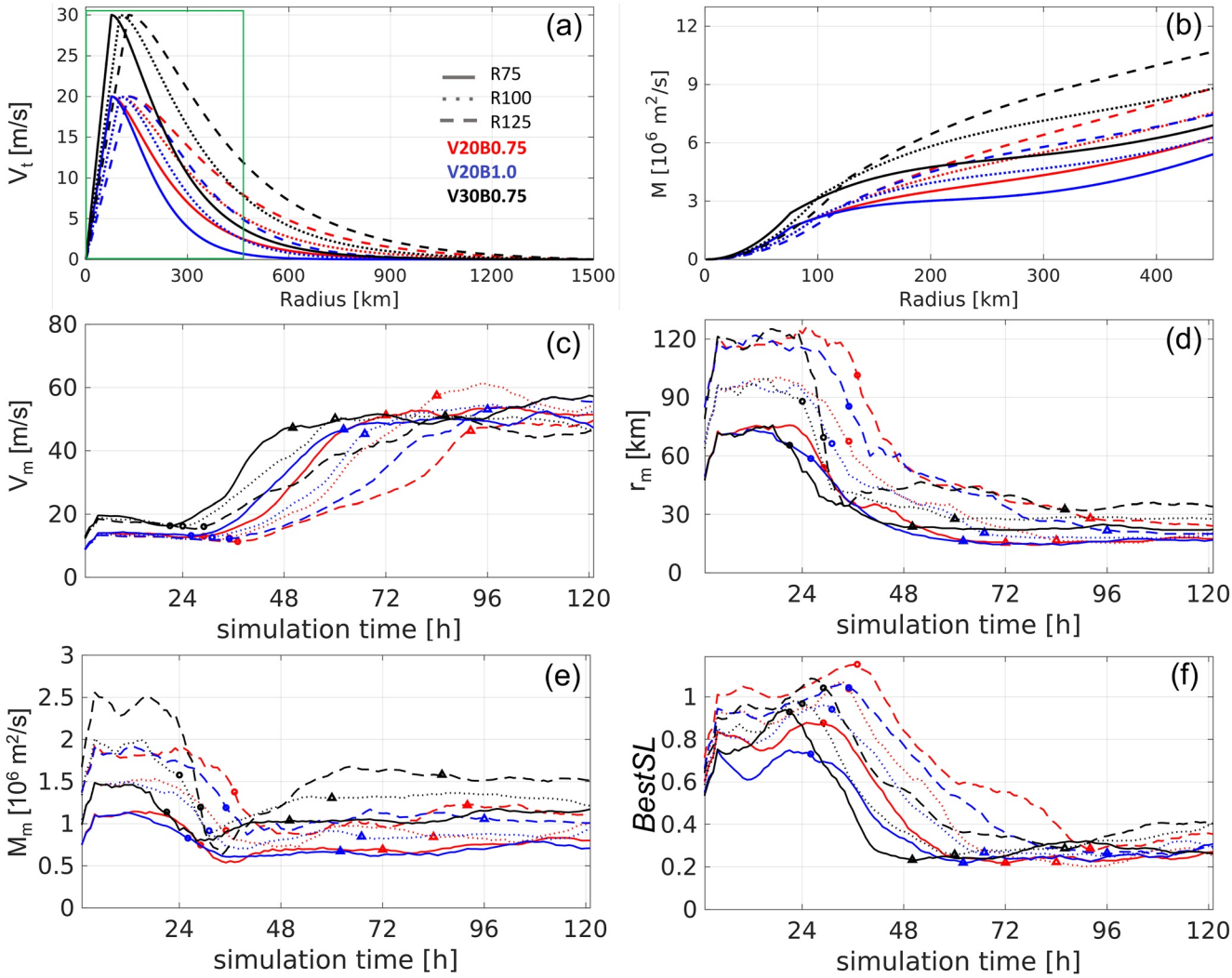


**Figure 1.** (a) Initial surface wind profiles and corresponding (b) initial inner-core M profiles. Time evolutions of (c) maximum azimuthally averaged 10-m tangential wind ($V_m$), (d) radius of $V_m$, (e) absolute angular momentum at $r_m$, and (f) BestSL, which is calculated using a best-linear-fit line that passes the point $r^* = 1$ and $M^* = 1$ and uses the points between $r^* = 1$ and $r^* = 2$ for $r_m >$ 60 km, between $r^* = 1$ and $r^* = 4$ for $r_m \leq 60$ km to ensure enough number of data points for the linear fit. The start (end) time of an RI period is marked by a circle (triangle).

To verify the broad validity of this quasi-linear $M$ slope assumption, we set up the simulations initialized with different storm structures. The radial profiles of the initial surface tangential winds from Equation 1 of Xu and Wang (2018) are shown in Figure 1a. There are three different initial $r_m$ values ($r_m$ = 75, 100, and 125 km) and two different "skirt" parameters ($B$ = 1.0 and 0.75; a smaller $B$ produces a broader radial profile). We also included a sensitivity group with stronger initial maximum tangential wind (30 $ms^{-1}$ vs. 20 $ms^{-1}$). With all the variations, there are nine simulations in total. The tangential wind vanishes at $r$ = 1,500 km. Figure 1b is the consequent $M$ profiles inside 450-km radius. As shown in Figure 1a, the V30B0.75 group has stronger winds outside of $r_m$, which in a sense falls into the large TC regime.

RI, as defined by the National Hurricane Center (NHC) glossary, is "an increase in the maximum sustained winds of a TC of at least 30 kt in a 24-hr period." This definition represents the 95th percentile of all over-water Atlantic basin intensification rates (Kaplan & DeMaria, 2003). However, this operational definition may not necessarily be the best to reflect the relevant physical processes under RI onset. For the simulations, we define RI onset as the point with the sharpest increase in 3-hr intensity change (marked by circles in Figures 1c–1f). The end of the RI period is defined similarly but with the sharpest decrease (marked by triangles in Figures 1c–1f). It is observed that all simulations have an adjustment period before RI onset and a quasi-steady state after RI (Figure 1c). The

evolutions of $r_m$ (Figure 1d) and $M_m$ (Figure 1e) show that a wide range of TC structures and sizes are achieved by using different initial wind profiles. The SL magnitudes calculated using best linear fitting (hereafter, BestSL) decrease monotonically during RI (Figure 1f). More details about the relationship among BestSL magnitudes, TC structure and intensity learned from the idealized simulations are presented in Section 3.1.

### 2.2. Extended Best-Track (EBT)

The EBT data set (Demuth et al., 2006) contains the maximum one-minute sustained surface wind speed ($V_m$), $r_m$, and radius of gale force wind ($r17$) in each storm quadrant every 6 hr for Atlantic TCs during the period of 1851–2020, although only TCs from 1988 onwards meet all the below criteria. Beginning with the entire EBT data set, strict quality control was used to select only (a) the records during RI using the NHC definition, (b) times during which $V_m$, $r_m$, and $r17$ are all available ($r17$ must be available in at least two quadrants and the average of $r17$ amongst the available quadrants was used), and (c) $V_m$ is at least 20 $ms^{-1}$ to avoid the early disorganized stage. Tao and Zhang (2019) pointed out that axisymmetric mode dominates TCs under RI, which partly secures the axisymmetric structure of the records used in the calculation. A total of 64 TCs between 1988 and 2020 meet the above criteria and a total of 492 samples of $V_m$, $r_m$, and $r17$ are available. Given $r_m$, $V_m$, and $r17$, we are able to calculate

$$\mathrm{SL17} = \left(\frac{M17}{M_m} - 1\right) \Big/ \left(\frac{r17}{r_m} - 1\right). \tag{5}$$

The EBT SL17 is then compared to the WRF simulated SL17.

## 3. Results

### 3.1. Structural Evolution of the Simulated TCs During RI

The WRF simulated 10-m azimuthally averaged tangential winds ($V_t$) as a function of radius during RI are presented in Figure 2, which shows that RI is predominantly an inner core process: the wind structure changes dramatically in the inner core, while the outer wind does not change much. It is also observed that $r_m$ decreases and $r17$ increases during RI for all setups. Meanwhile, the area of changing winds is dependent on the vortex size such that $r17$ increases the most in the largest storm V30B0.75R125 compared to the smallest increase in the smallest storm V20B1.0R75.

The radial profiles of $M$ (Figure 3) evolve correspondingly to $V_t$. The outer larger $M$ values gradually fill up the inner core, which is consistent with the inward advection of the larger $M$ by the radial inflow. The relative change between $r_m$ and $r17$ is clearly dependent on TC size, as indicated by larger distances between the $r_m$ and $r17$ markers for larger TCs.

As shown in Figures 2 and 3, TC structures can vary greatly during RI and among different storms, which result in difficulties in finding an intensity-size relationship and developing a universal TC structure model in the physical space. Meanwhile, the BestSL color coding shows similarities among different structural changes in $V_t(r)$ and $M(r)$.

In the coordinate normalized by $r_m$ and $V_m$, as shown in Figure 4e, the WRF simulated $V^*(r^*)$ profiles have intersections of different profiles outside $r^* = 2$. The profiles between $r^* = 1$ and $r^* = 2$ have better orders such that stronger storms (cold colors) have faster wind reduction and weaker storms (warm colors) have slower wind reduction right outside $r^* = 1$. In contrast to the complicated simulated $V^*(r^*)$ profiles, Figure 4a presents a sequence of BestSL values in simulated $M^*(r^*)$ profiles. From Figure 1f and the color codes in Figure 2, the BestSL values show a dependence on intensity. In general, larger $V_m$ corresponds with smaller BestSL values (Figures 1f and 2) and flatter $M^*$ slopes (Figure 4a) as well as sharper decreases in $V^*$ outside $r^* = 1$ (Figure 4e).

All WRF simulated TCs in this study behave similarly in terms of $M^*(r^*)$. Due to the aircraft data coverage issue, Martinez et al. (2017) only showed that the structure of absolute angular momentum surfaces outside $r^* = 1$ is quasi-linear out to $r^* = 4$. In the simulations shown in Figure 4a, this quasi-linear slope assumption is valid well beyond $r^* = 4$. Interestingly, the $M^*(r)$ structure inside $r^* = 1$ also shows some intensity relationship (Figure 4a) such that weaker storms have $M^* \sim r^*$ while stronger storms have $M^* \sim r^{*\beta}$ where $\beta > 1$. An explanation for this structure inside $r^* = 1$ is beyond the scope of this study.

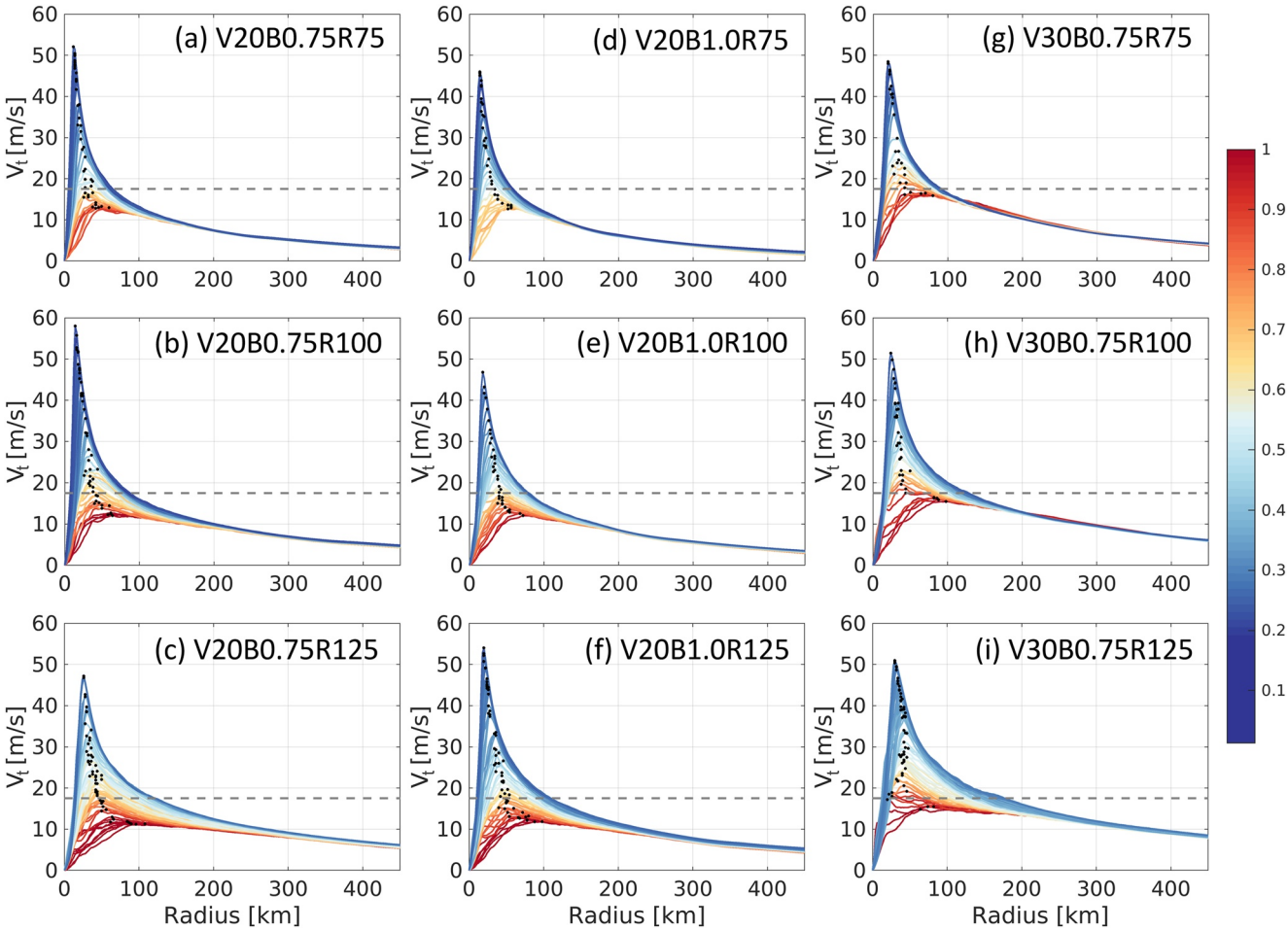


**Figure 2.** The hourly evolution of $V_t(r)$ during each RI period. Color coded by BestSL values from Figure 1f. The gray dash lines indicate 17.5 $ms^{-1}$ and the black dots indicate $r_m$.

### 3.2. Comparison Among SL Model, mRankine Model and C15 Model Results

In this section, we compared the WRF simulated wind structures to the ones obtained from the SL, mRankine, and C15 models. As $r_m$, $V_m$, and $r17$ are routine records in TC observations, they are the only inputs from the WRF simulations that are taken by the SL and mRankine models, while the C15 model only needs two inputs ($r_m$, $V_m$).

In the SL model, SL17 is calculated using Equation 5 and then $V_t$ is calculated from Equation 4. In the mRankine model, $\alpha = \frac{\log(17.5/V_m)}{\log(r_m/r17)}$ such that the fitted profile intersects point [$r_m$, $V_m$] and point [$r17$, 17.5 $ms^{-1}$]. Once an $\alpha$ value is found for one WRF simulated wind profile, the mRankine fitted $V_t$ is calculated using Equation 1.

The complete C15 wind profiles are calculated by using the C15 code (Chavas, 2022) which merges inner-core wind profiles with outer-core wind profiles. The inner-core profile of the C15 model is shown in Equation 2, which gives one $M^*(r^*)$ with one $C_k/C_d$ value. The magnitude of $C_k/C_d$ is from C15: $\frac{C_k}{C_d} = 0.00055{V_m}^2 - 0.0259V_m + 0.763$. The outer-core wind is determined by $\frac{\partial M}{\partial r} = \frac{2C_d}{W_{cool}} \frac{(rV)^2}{{r_0}^2 - r^2}$, where the parameter $W_{cool} = 2$ $mms^{-1}$ is the radiative-subsidence rate, $C_d$ uses the format in Donelan et al. (2004), $r_0$ is the radius where $V_t$ becomes zero. More details can be found in C15 and Chavas (2022).

Among the three wind structure models, the SL model performs the best as it captures the range of $M^*(r^*)$ at all $r^*$ as well as the shape of individual $M^*(r^*)$ profiles as seen in Figures 4a–4d. The mRankine model generally performs well except for the larger curvature especially in weak TCs (red colored lines). The C15 model generates

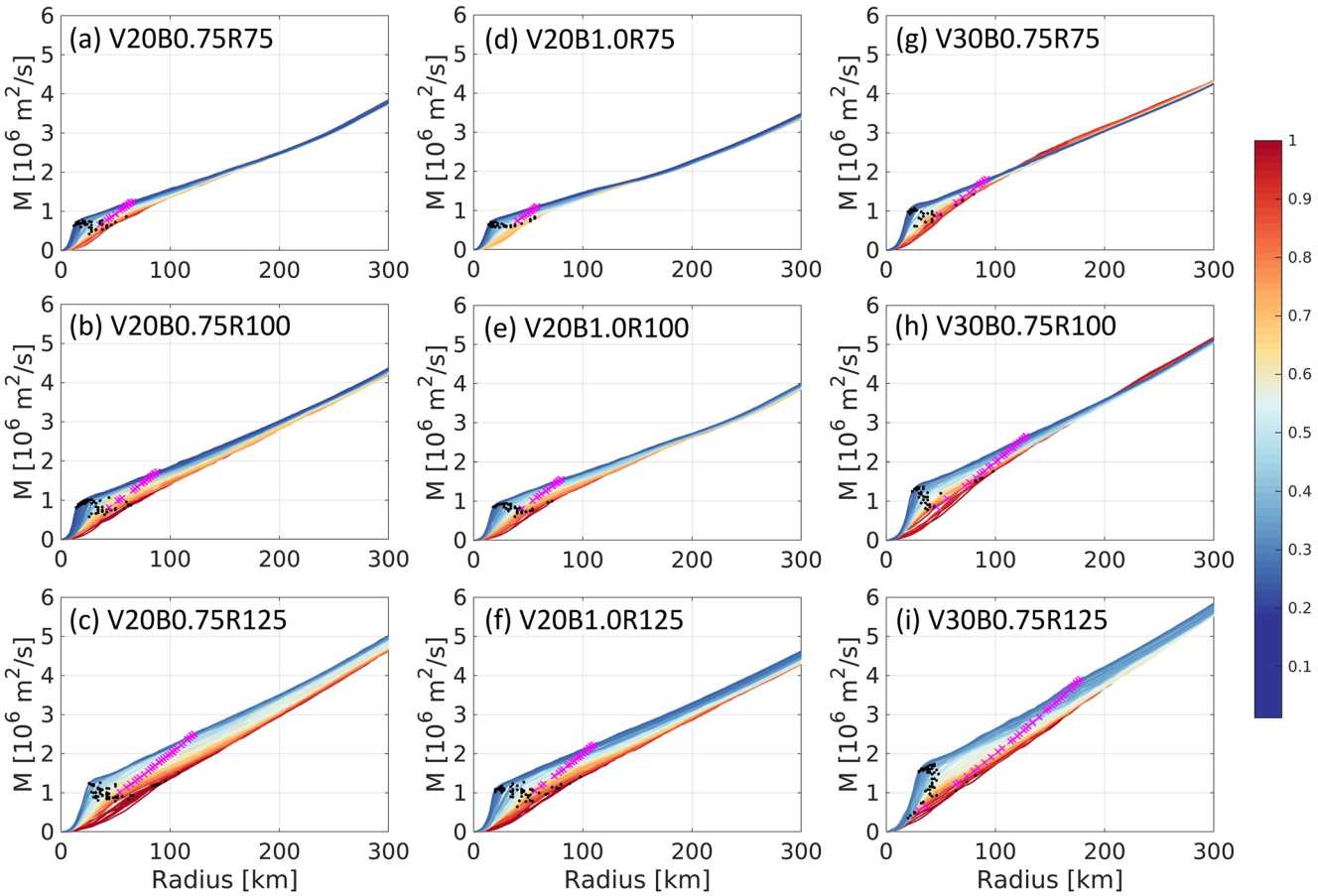


**Figure 3.** Similar to Figure 2 but for $M(r)$. Color coded by BestSL values from Figure 1f. The magenta crosses indicate $r17$ and the black dots indicate $r_m$.

little variation between $r^* = 1$–2 such that the consequent outer-core profiles also show a narrow $M^*(r^*)$ range. This little variation in the inner core of the C15 model is also pointed out in Chavas and Lin (2016).

The SL model also stands out among the comparison of $V^*(r^*)$ profiles as it captures not only the range but also the intersections among profiles as shown in Figure 4e. The mRankine $V^*(r^*)$ profiles shown in Figure 4g have no intersections among profiles with different $\alpha$ values. Meanwhile, the C15 $V^*(r^*)$ profiles shown in Figure 4h have little variability especially in the inner core.

The errors between the wind structure models and the WRF simulated wind profiles are shown in the last two columns of Figure 4. Among the three wind structure models, the SL model and the mRankine model perform better than the C15 model between $r^* = 1$–3, while the C15 model has a quite good fit at the radii beyond $r^* = 4$. The mRankine model works quite well for strong TCs, while the error at large radii is biased on the positive side especially for weak TCs. In contrast, the C15 model has a positive bias for strong TCs, a negative bias for weak TCs and a good fit for intermediate TCs. It's worth noting that the errors from the C15 outer wind model flatten out to large radii, which indicates that the outer wind model performs well but retains the errors induced by the inner wind model (Figures 4k & 4n).

Generally speaking, the SL model performs well in representing the WRF simulated wind profiles given minimal information at point [$r_m$, $V_m$] and point [$r17$, 17.5 ms$^{-1}$] and the simple reconstruction process.

### 3.3. Comparison Among WRF SL17, EBT SL17 and WRF BestSL

From Section 3.2, we have shown that using SL17 calculated using $r_m$, $V_m$, and $r17$ from the WRF simulations, the SL model captures the WRF simulated inner-core wind structure quite well. To assure that this SL17 is representative for real TCs, we calculated SL17 from the EBT data set for all Atlantic TC RI events since 1988. Though

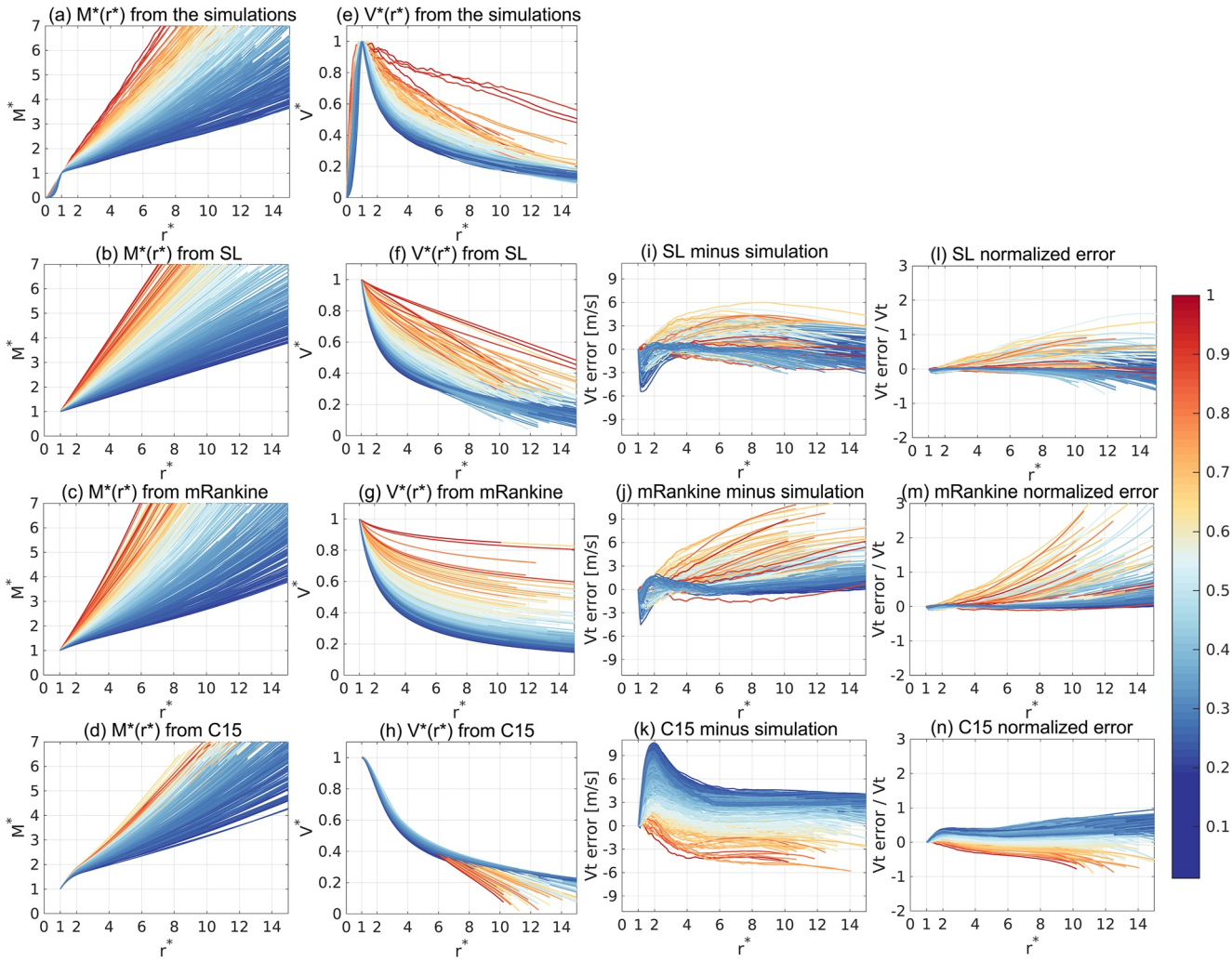


**Figure 4.** First row: results from all WRF model simulations during RI when Vmax > 17.5 $ms^{-1}$; second row: fitted profiles using SL model; third row: fitted profiles using mRankine model; fourth row: fitted profiles using C15 model. (a–d) $M^*(r^*)$; (e–h) $V^*(r^*)$; (i–k) $V_t$ error between wind structure model results and WRF simulated profiles; (l–n) $V_t$ error normalized by the WRF simulated $V_t$ at the same radius. All lines are color-coded by BestSL values in Figure 1f.

there is a spread of SL17 for a given $V_m$ value, SL17 decreases with increasing $V_m$ (Figure 5a). The SL17 values calculated from the WRF simulations overlap with the SL17 values calculated from the EBT, which implies that real TCs may also have a quasi-linear absolute angular momentum slope during RI and this linear slope flattens with intensification. A power function fit to the model simulated SL17 values gives

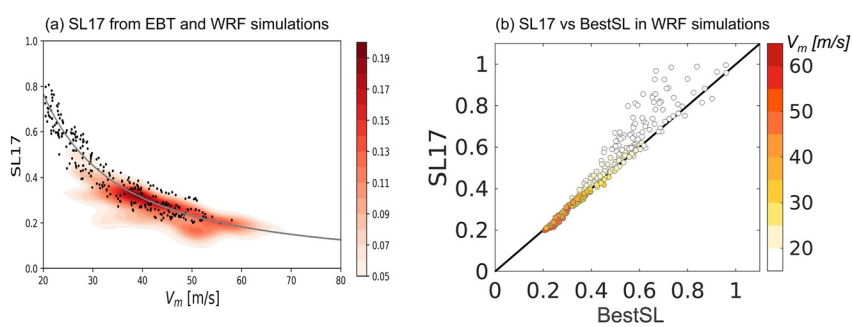


**Figure 5.** (a) Kernel density plot of SL17 during RI from EBT data set (shading); black dots depict SL17 from WRF simulations and gray curve represents power function fit to WRF simulated SL17. (b) WRF simulated SL17 plotted against BestSL, color-coded by $V_m$.

$$SL17 = 38.33 \times V_m^{-1.31} \quad (6)$$

which well describes SL17 in both the model simulations and observations.

We note that SL17 in EBT has a quite large spread for a given intensity, especially for low $V_m$ values. This spread is partially because EBT contains TCs with different maximum potential intensities from different environmental conditions. Nevertheless, the good fit between WRF simulated SL17 and EBT SL17 partially confirms that the findings from the idealized model simulations can be extended to observed TCs.

Figure 5b reassures the representativeness of SL17 for the BestSL values calculated from the best linear fit as shown in Figure 1f. SL17 tends to be larger than BestSL when $V_m < 20$ ms$^{-1}$, which is reasonable as point [$r_m$, $V_m$] and point [$r17$, 17.5 ms$^{-1}$] are too close to well represent the overall wind structure outside $r_m$. For $V_m > 20$ ms$^{-1}$, SL17 is almost equal to BestSL which gives confidence in using SL17 to reconstruct wind profiles outside $r_m$.

## 4. Conclusions and Discussion

This study confirms the hypotheses of the quasi-linear $M$ slope outside of $r_m$ from idealized simulations and the relationship between the non-dimensional $M$ slope and TC intensity from both the idealized WRF simulations and the EBT data set. For a well-organized TC during RI, the normalized quasi-linear $M$ slope outside of $r_m$ flattens with increasing intensity.

The introduction of the SL model provides a simple solution to reconstruct continuous wind profiles outside $r_m$. Practically, using $r_m$, $V_m$, $r17$, which are all available from operational estimates, and Equation 4, the full profile of $V_t(r)$ can be reconstructed. We believe that the simplicity of Equation 4 and good fit using the SL model for WRF simulated wind profiles show great prospects for future applications, such as validating simulations/data assimilation updates, providing wind profiles for storm surge calculations, and issuing high-wind warnings.

Despite the benefits from using linear $M$ slope assumptions, it is worth mentioning the caveats: the linear slope assumption may not behave well for TCs under strong asymmetry (e.g., weak, disorganized, or tilted TCs). Since this linear slope is found from an empirical approach, we expect other model simulations or observations can provide confirmation across a wider range of conditions.

## Data Availability Statement

Extended best-track data set: https://rammb2.cira.colostate.edu/research/tropical-cyclones/tc_extended_best_track_dataset/. The 10-m wind data from the WRF simulations: https://doi.org/10.5281/zenodo.8134201. The code used to calculate the complete C15 wind profiles: https://purr.purdue.edu/publications/4066/1.

**Acknowledgments**
Drs. D. Tao and M. Bell are supported by Office of Naval Research award N000142012069. Dr. R. Nystrom is supported by the Advanced Study Program in the National Center for Atmospheric Research which is a major facility sponsored by the National Science Foundation under Cooperative Agreement 1852977. Computing was conducted on Supercomputer Stampede2 of the Texas Advanced Computing Center (TACC). We would like to thank Dr. Dan Chavas and another reviewer for the insightful review comments.

## References

Braun, S. A., Sippel, J. A., & Nolan, D. S. (2012). The impact of dry midlevel air on hurricane intensity in idealized simulations with no mean flow. *Journal of the Atmospheric Sciences*, *69*(1), 236–257. https://doi.org/10.1175/JAS-D-10-05007.1

Casas, E., Tao, D., & Bell, M. (2023). An intensity and size phase space for tropical cyclone structure and evolution. *Journal of Geophysical Research: Atmosphere*, *128*(4), e2022JD037089. https://doi.org/10.1029/2022JD037089

Chavas, D. R. (2022). *Code for tropical cyclone wind profile model of Chavas et al (2015, JAS)*. Purdue University Research Repository. https://doi.org/10.4231/CZ4P-D448

Chavas, D. R., & Knaff, J. A. (2022). A simple model for predicting the tropical cyclone radius of maximum wind from outer size. *Weather and Forecasting*, *37*(5), 563–579. https://doi.org/10.1175/WAF-D-21-0103.1

Chavas, D. R., & Lin, N. (2016). A model for the complete radial structure of the tropical cyclone wind field. Part II: Wind field variability. *Journal of the Atmospheric Sciences*, *73*(8), 3093–3113. https://doi.org/10.1175/JAS-D-15-0185.1

Chavas, D. R., Lin, N., & Emanuel, K. (2015). A model for the complete radial structure of the tropical cyclone wind field. Part I: Comparison with observed structure. *Journal of the Atmospheric Sciences*, *72*(9), 3647–3662. https://doi.org/10.1175/JAS-D-15-0014.1

Christophersen, H., Sippel, J., Aksoy, A., & Baker, N. L. (2022). Recent advancements for tropical cyclone data assimilation. *Annals of the New York Academy of Sciences*, *1517*(1), 25–43. https://doi.org/10.1111/nyas.14873

DeMaria, M., Knaff, J. A., Knabb, R., Lauer, C., Sampson, C. R., & DeMaria, R. T. (2009). A new method for estimating tropical cyclone wind speed probabilities. *Weather and Forecasting*, *24*(6), 1573–1591. https://doi.org/10.1175/2009WAF2222286.1

Demuth, J. L., DeMaria, M., & Knaff, J. A. (2006). Improvement of advanced microwave sounding unit tropical cyclone intensity and size estimation algorithms. *Journal of Applied Meteorology and Climatology*, *45*(11), 1573–1581. https://doi.org/10.1175/JAM2429.1

Donelan, M. A., Haus, B. K., Reul, N., Plant, W. J., Stiassnie, M., & GraberSaltzman, H. C. E. S. (2004). On the limiting aerodynamic roughness of the ocean in very strong winds. *Geophysical Research Letters*, *31*(18), L18306. https://doi.org/10.1029/2004gl019460

Dudhia, J., & Coauthors (2008). Prediction of Atlantic tropical cyclones with the advanced hurricane WRF (AHW) model. In *Preprints, 28th conf. on hurricanes and tropical meteorology*. Amer. Meteor. Soc. 18A.2 Retrieved from https://ams.confex.com/ams/28Hurricanes/techprogram/paper_138004.htm

Dunion, J. P., & Marron, C. S. (2008). A reexamination of the Jordan mean tropical sounding based on awareness of the Saharan air layer: Results from 2002. *Journal of Climate*, *21*(20), 5242–5253. https://doi.org/10.1175/2008JCLI1868.1

Emanuel, K. A. (2004). In E. Fedorovich, R. Rotunno, & B. Stevens (Eds.), *Tropical cyclone energetics and structure. Atmospheric turbulence and mesoscale meteorology* (pp. 165–192). Cambridge University Press.

Emanuel, K. A., & Rotunno, R. (2011). Self-stratification of tropical cyclone outflow. Part I: Implications for storm structure. *Journal of the Atmospheric Sciences*, *68*(10), 2236–2249. https://doi.org/10.1175/JAS-D-10-05024.1

Holland, G. J. (1980). An analytic model of the wind and pressure profiles in hurricanes. *Monthly Weather Review*, *108*(8), 1212–1218. https://doi.org/10.1175/1520-0493(1980)108<1212:AAMOTW>2.0.CO;2

Hong, S.-Y., & Lim, J.-O. J. (2006). The WRF single-moment 6-class microphysics scheme (WSM6). *Journal of the Korean Meteorological Society*, *42*, 129–151.

Hong, S.-Y., Noh, Y., & Dudhia, J. (2006). A new vertical diffusion package with an explicit treatment of entrainment processes. *Monthly Weather Review*, *134*(9), 2318–2341. https://doi.org/10.1175/MWR3199.1

Kaplan, J., & DeMaria, M. (2003). Large-scale characteristics of rapidly intensifying tropical cyclones in the North Atlantic Basin. *Weather and Forecasting*, *18*(6), 1093–1108. https://doi.org/10.1175/1520-0434(2003)018<1093:LCORIT>2.0.CO;2

Klotzbach, P. J., Chavas, D. R., Bell, M. M., Bowen, S. G., Gibney, E. J., & Schreck, C. J., III. (2022). Characterizing continental US hurricane risk: Which intensity metric is best? *Journal of Geophysical Research: Atmospheres*, *127*(18), e2022JD037030. https://doi.org/10.1029/2022JD037030

Knaff, J. A., Sampson, C. R., Kucas, M. E., Slocum, C. J., Brennan, M. J., Meissner, T., et al. (2021). Estimating tropical cyclone surface winds: Current status, emerging technologies, historical evolution, and a look to the future. *Tropical Cyclone Research and Review*, *10*(3), 125–150. https://doi.org/10.1016/j.tcrr.2021.09.002

Knaff, J. A., Slocum, C. J., Musgrave, K. D., Sampson, C. R., & Strahl, B. R. (2016). Using routinely available information to estimate tropical cyclone wind structure. *Monthly Weather Review*, *144*(4), 1233–1247. https://doi.org/10.1175/MWR-D-15-0267.1

Komaromi, W. A., Reinecke, P. A., Doyle, J. D., & Moskaitis, J. R. (2021). The naval research laboratory's coupled ocean–Atmosphere mesoscale prediction system-tropical cyclone ensemble (COAMPS-TC ensemble). *Weather and Forecasting*, *36*(2), 499–517. https://doi.org/10.1175/WAF-D-20-0038.1

Mallen, K. J., Montgomery, M. T., & Wang, B. (2005). Reexamining the near-core radial structure of the tropical cyclone primary circulation: Implications for vortex resiliency. *Journal of the Atmospheric Sciences*, *62*(2), 408–425. https://doi.org/10.1175/JAS-3377.1

Martinez, J., Bell, M. M., Vigh, J. L., & Rogers, R. F. (2017). Examining tropical cyclone structure and intensification with the FLIGHT+ dataset from 1999 to 2012. *Monthly Weather Review*, *145*(11), 4401–4421. https://doi.org/10.1175/MWR-D-17-0011.1

Nystrom, R. G., Rotunno, R., Davis, C. A., & Zhang, F. (2020). Consistent impacts of surface enthalpy and drag coefficient uncertainty between an analytical model and simulated tropical cyclone maximum intensity and storm structure. *Journal of the Atmospheric Sciences*, *77*(9), 3059–3080. https://doi.org/10.1175/JAS-D-19-0357.1

Rappin, E. D., Nolan, D. S., & Majumdar, S. J. (2013). A highly configurable vortex initialization method for tropical cyclones. *Monthly Weather Review*, *141*(10), 3556–3575. https://doi.org/10.1175/MWR-D-12-00266.1

Stern, D. P., & Nolan, D. S. (2012). On the height of the warm core in tropical cyclones. *Journal of the Atmospheric Sciences*, *69*(5), 1657–1680. https://doi.org/10.1175/JAS-D-11-010.1

Tao, D., van Leeuwen, P. J., Bell, M., & Ying, Y. (2022). Dynamics and predictability of tropical cyclone rapid intensification in ensemble simulations of Hurricane Patricia (2015). *Journal of Geophysical Research: Atmospheres*, *127*, e2021JD036079. https://doi.org/10.1029/2021JD036079

Tao, D., & Zhang, F. (2019). Evolution of dynamic and thermodynamic structures before and during rapid intensification of tropical cyclones: Sensitivity to vertical wind shear. *Monthly Weather Review*, *147*(4), 1171–1191. https://doi.org/10.1175/MWR-D-18-0173.1

Willoughby, H., Darling, R., & Rahn, M. (2006). Parametric representation of the primary hurricane vortex. Part II: A new family of sectionally continuous profiles. *Monthly Weather Review*, *134*(4), 1102–1120. https://doi.org/10.1175/MWR3106.1

Xu, J., & Wang, Y. (2018). Effect of the initial vortex structure on intensification of a numerically simulated tropical cyclone. *Journal of the Meteorological Society of Japan*, *96*(2), 111–126. https://doi.org/10.2151/jmsj.2018-014

Yan, D. C., & Zhang, T. Y. (2022). Research progress on tropical cyclone parametric wind field models and their application. *Regional Studies in Marine Science*, *51*, 102207. https://doi.org/10.1016/j.rsma.2022.102207